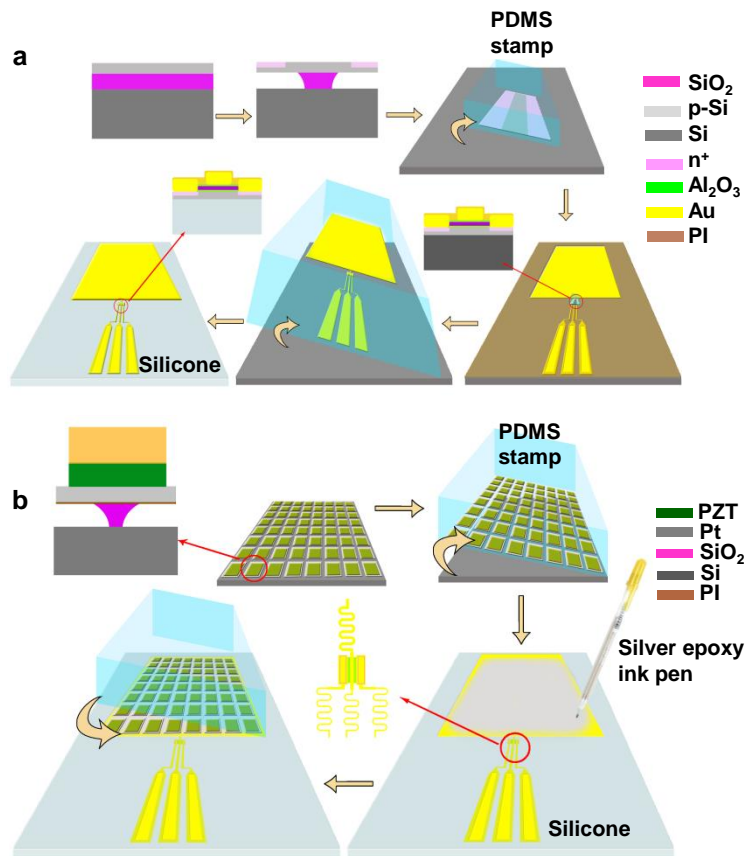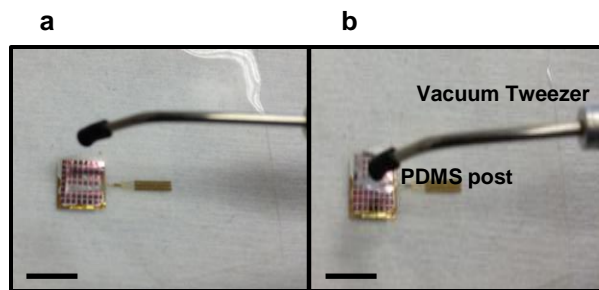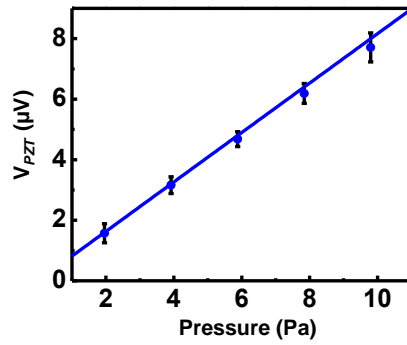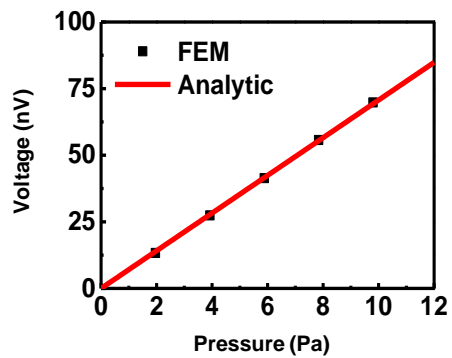**Supplementary Figures**

Supplementary Figure 1| Device layouts and fabrication steps of PZT pressure sensors and printed SiNM n-MOSFETs on a silicone substrate. Schematic illustration of fabrication steps of **(a)** SiNM n-MOSFET, **(b)** PZT sensors.

Supplementary Figure 2| Method for applying pressure to a device with a PDMS post. Photograph of a PDMS post on the pressure sensor, (**a**) released from and (**b**) held by a vacuum tweezer. The scale bars are 1cm.

Supplementary Figure 3| Measurement repeatability. Summary of data collected from multiple (50) measurements of the dependence of V_{PZT} on applied pressure for a sensor on silicone. The error bars correspond to the calculated standard error.

Supplementary Figure 4| Comparison between analytical and FEM results. Comparison of voltage vs. pressure obtained by analytical modeling and FEM for PZT sensors on a Si wafer substrate**.**
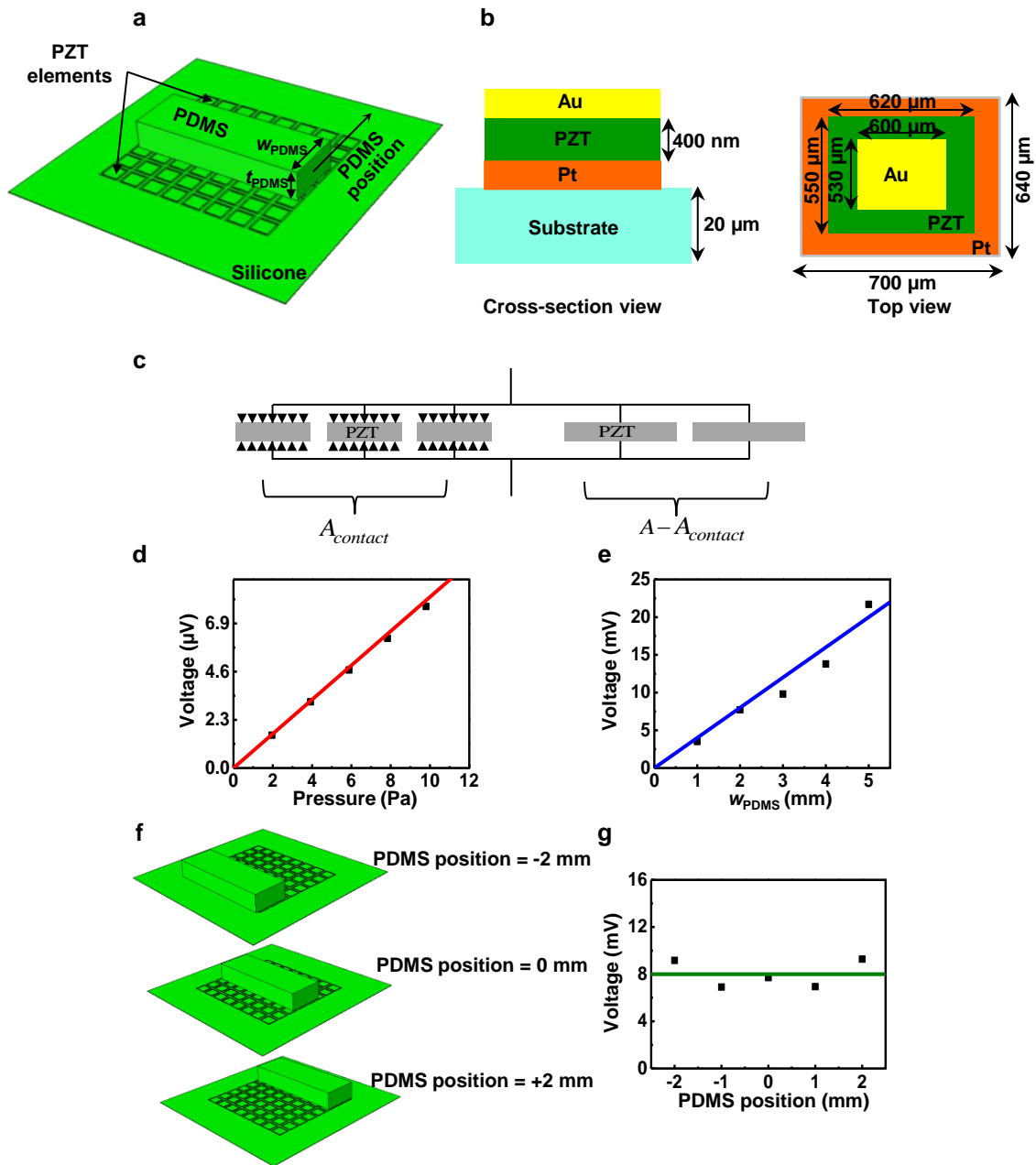
Supplementary Figure 5| Sensor layout and pressure application via a PDMS post. Schematic illustration of (**a**) pressure application via a PDMS post on a PZT sensor, (**b**) cross sectional and top views of a single PZT element, (**c**) pressed and unpressed regions of an array of PZT elements. Effects of (**d**) pressure, (**e**) width and (**f, g**) position on the output voltage for the PZT sensor on a silicone substrate.
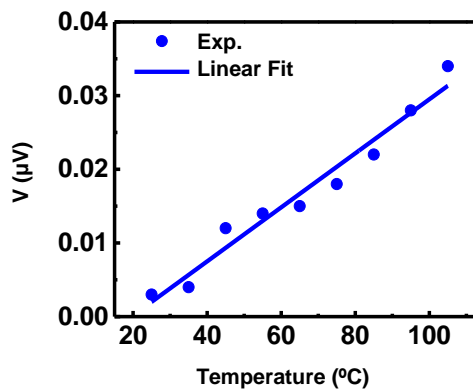
Supplementary Figure 6| The responses of the PZT elements associated with the pyroelectric effect. Dependence of the output voltage on the applied temperature.
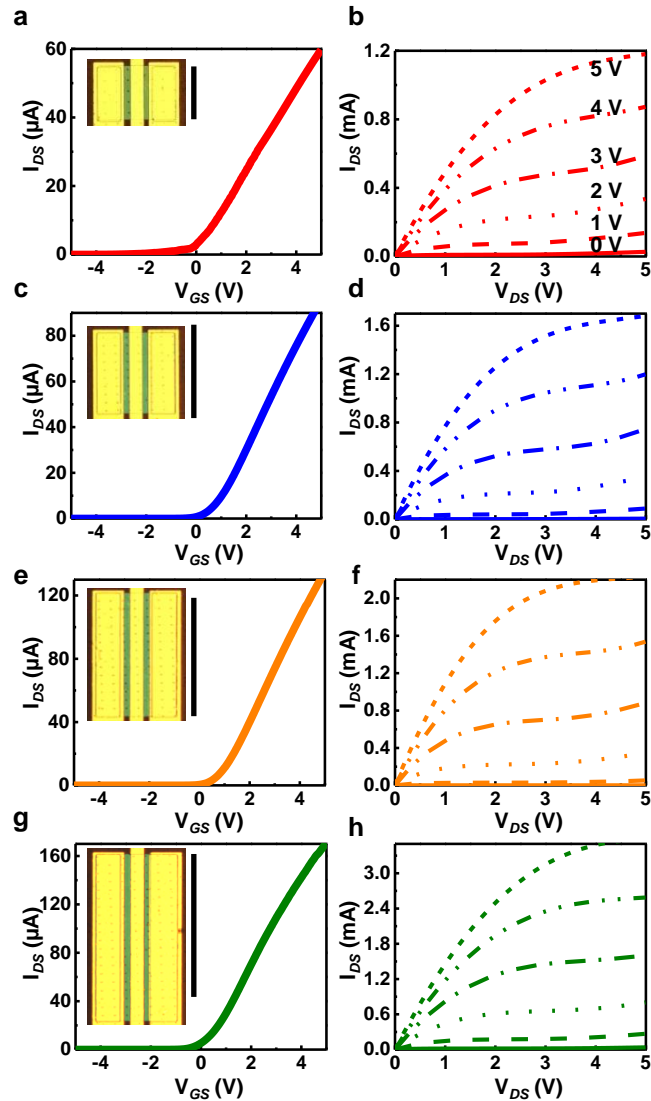
Supplementary Figure 7| Characterization of results for SiNM n-MOSFETs. (a,c,e,g) I_{DS} - V_{GS} characteristics of SiNM n-MOSFETs with 200 μm, 400 μm, 600 μm, 800 μm channel widths, respectively. The insets show microscope images of the devices. **(b,d,f,h)** I_{DS} - V_{DS} characteristics at constant V_G for SiNM n-MOSFETs with 200 μm, 400 μm, 600 μm, 800 μm channel widths, respectively. The scale bar is **(a)** 200 μm, **(c)** 400 μm, **(e)** 600 μm, **(g)** 800 μm.
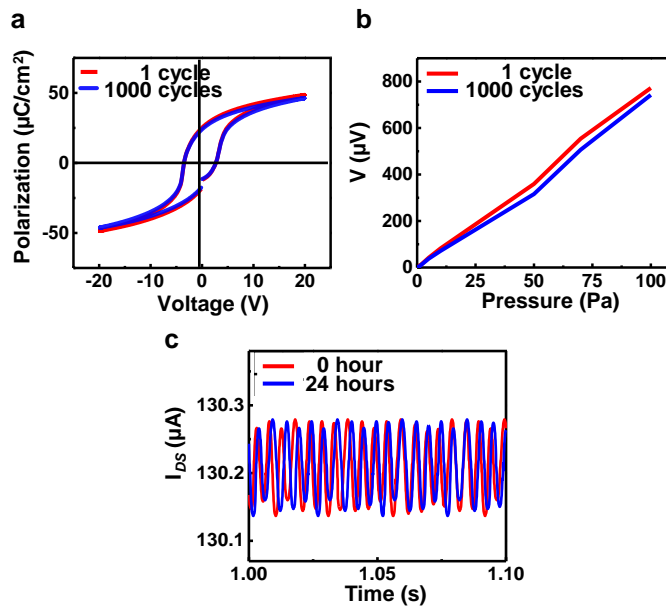
Supplementary Figure 8| Cycling Tests. (a) Polarization vs. voltage for the PZT sensor after 1 and 1000 cycles of applied pressure (10 Pa). **(b)** The voltage output of a PZT sensor after 1000 cycles of applied pressure. **(c)** The response of sensor with a SiNM n-MOSFET with a 800 μm channel width under iHM79 stereo speaker playing sound at 80 dB, 1 kHz for 24 hours.
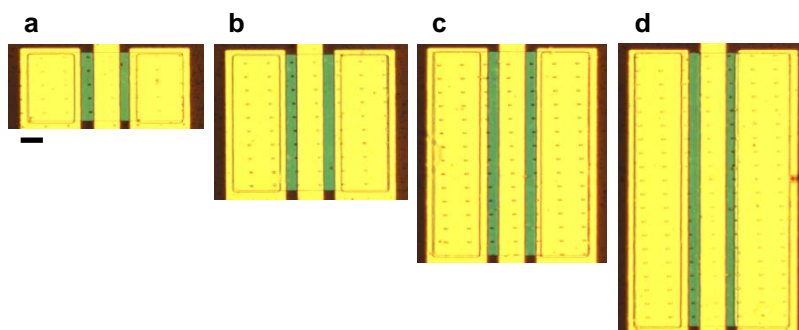
Supplementary Figure 9| Images of SiNM n-MOSFETs with various channel width. (a-d) Optical microscope images of SiNM n-MOSFETs with 200 μm, 400 μm, 600 μm, 800 μm channel width, respectively. The scale bar is 50 μm.
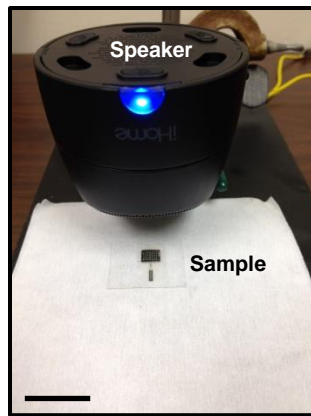
Supplementary Figure 10| Microphone test. Photograph of a sensor positioned ~1 cm away from an iHM79 stereo speaker while applying audible tones. The scale bar is 1 cm.
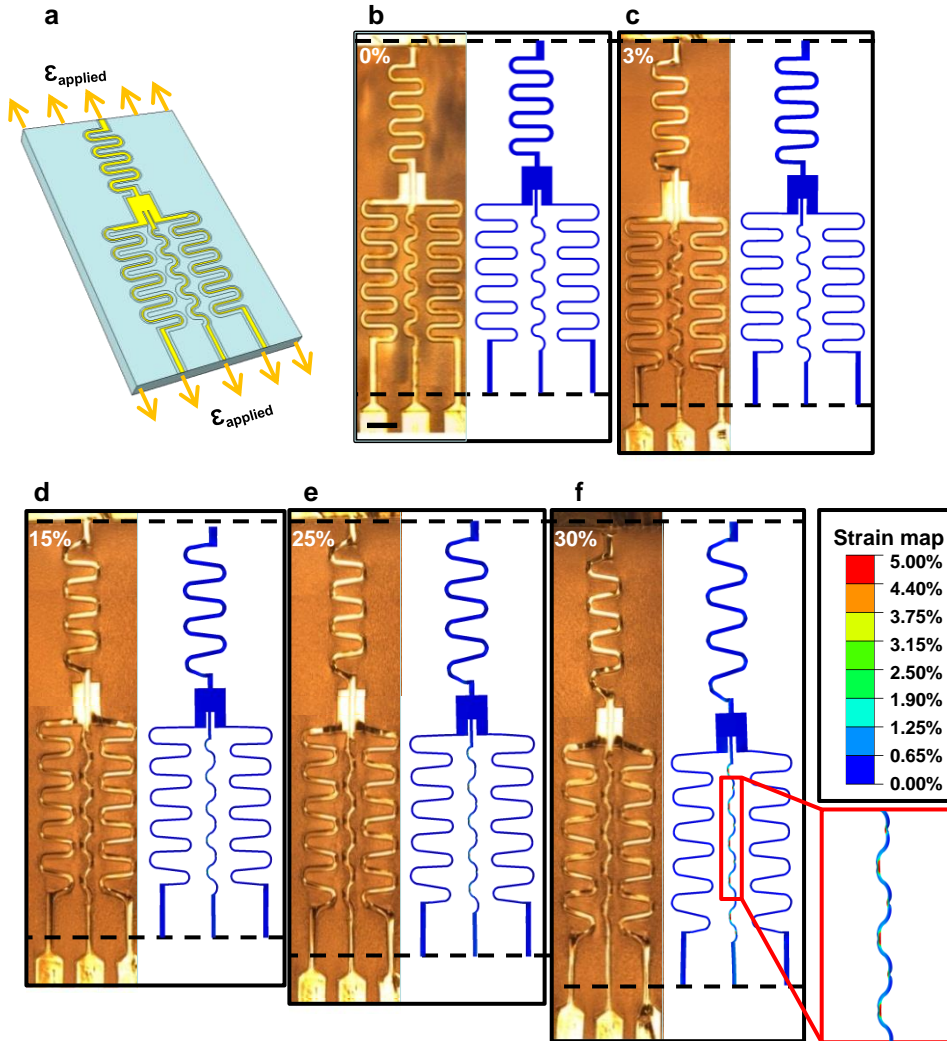
Supplementary Figure 11| Demonstration of stretchability in the pressure sensor. (a) Illustration of the model for FEM. **(b-f)** Optical images and corresponding FEM results for various levels of applied tensile strain. The color in the FEM plots represents the maximum principal strains in the metal layer. The scale bar is 300 μm.

a

b
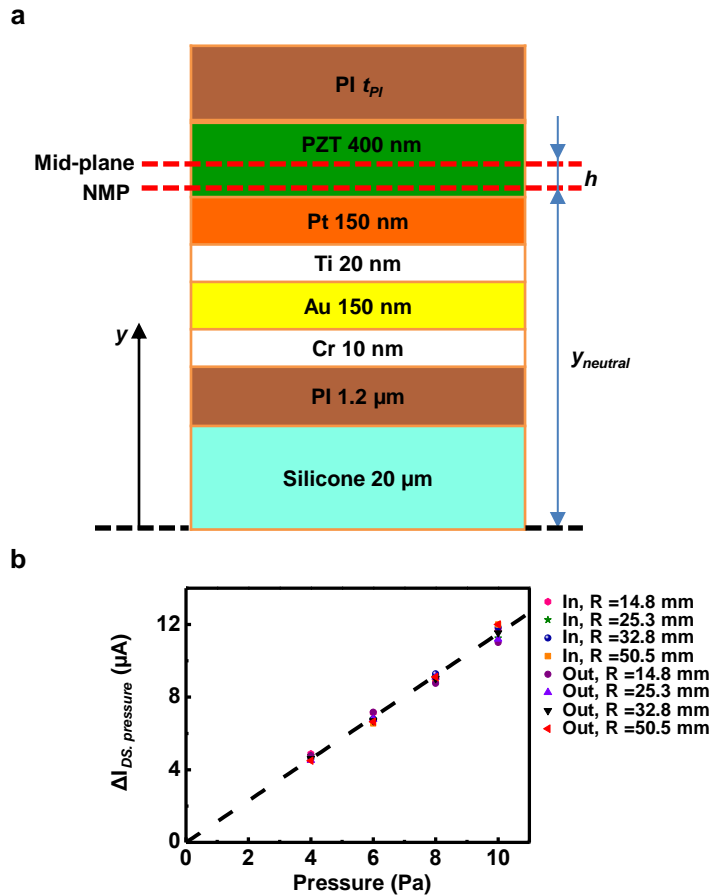
Supplementary Figure 12| Illustration of the neutral mechanical plane (NMP). (a) Schematic illustration of a PZT sensor on a silicone substrate with the NMP indicated. **(b)** ΔI_{DS} – Pressure for the sensor without a top coating PI, for different bending radii and direction; Inward (In) and Outward (Out). The device uses a SiNM n-MOSFET with 800 µm channel width.
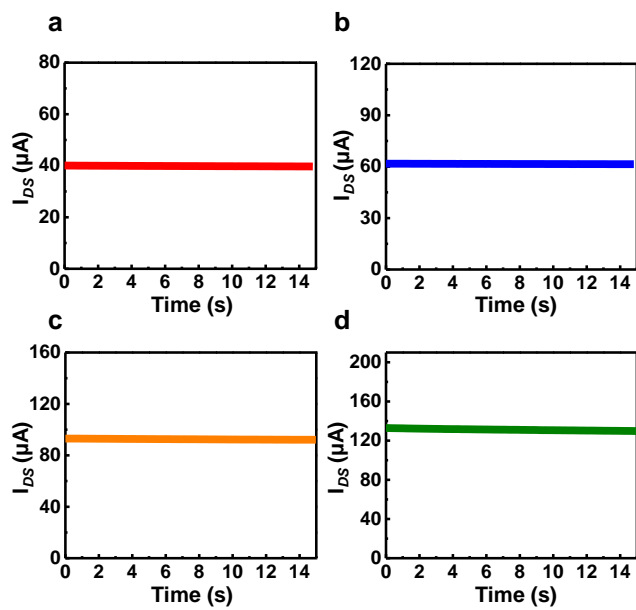
Supplementary Figure 13| The response of SiNM n-MOSFETs without pressure. (a-d) I_{DS} - Time plots for SiNM n-MOSFETs with 200 μm, 400 μm, 600 μm, 800 μm channel width, respectively, without applied pressure.
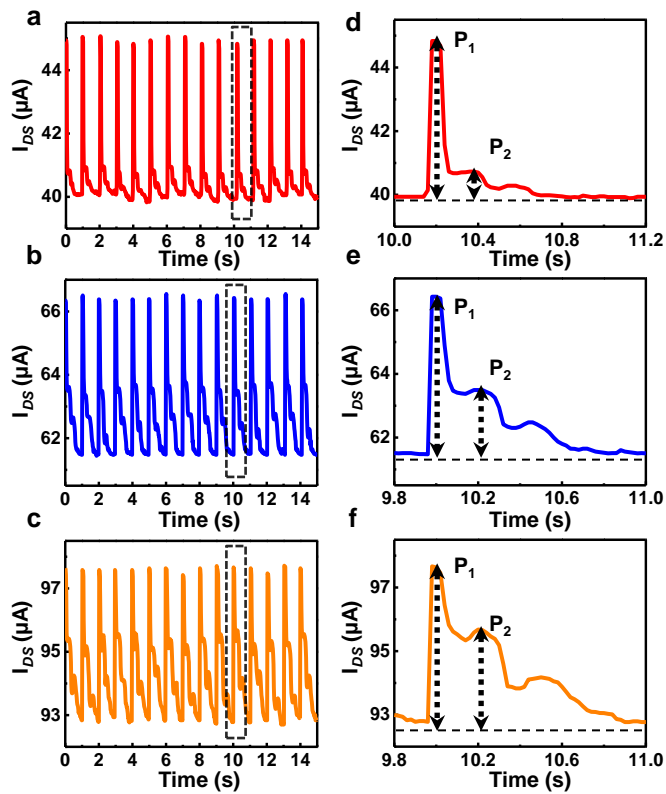
Supplementary Figure 14| Blood pressure wave pulse measurement. (a-c) I_{DS} - Time plots for the sensor with SiNM n-MOSFET with 400 μm, 600 μm, 800 μm channel width respectively under blood pressure effect on the wrist. **(d-f)** The peak in dashed rectangular region of **a-c** for the pressure sensor with SiNM n-MOSFET with 400 μm, 600 μm, 800 μm channel width, respectively, under blood pressure pulse effect on the wrist.
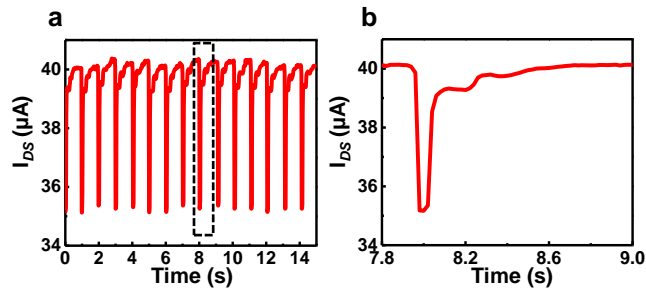
Supplementary Figure 15| Reverse poling effect on device response. (a) I_{DS} - Time plot for a sensor with a SiNM n-MOSFET that has 200 μm channel width and opposite poled PZT, responding to the effect of blood pressure measured on the wrist. **(b)** The peak in dashed rectangular region of **a**.
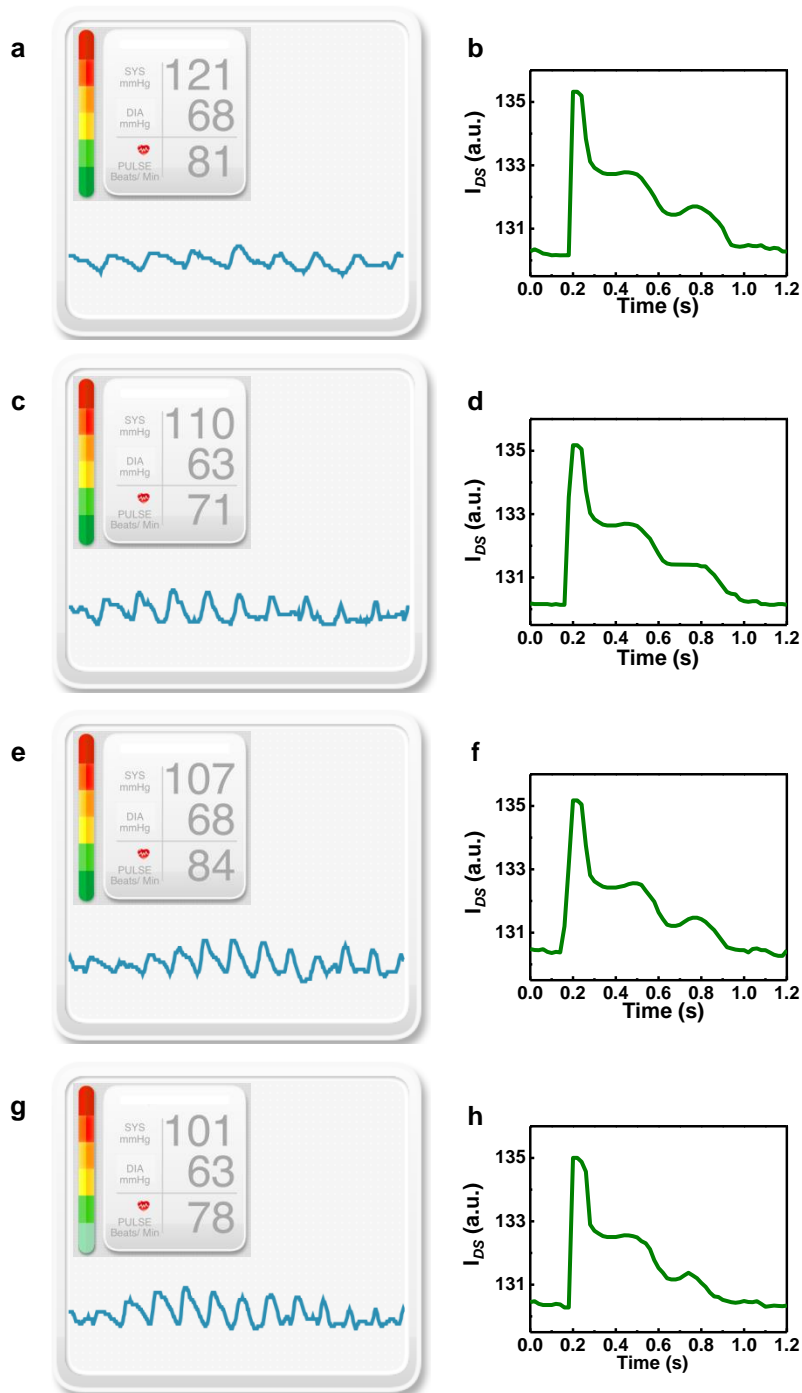
Supplementary Figure 16| Long term blood pressure monitoring via Blood Pressure Dock BP3 iHealth Lab Inc. and a sensor with a SiNM n-MOSFET with 800 μm channel width. (a,c,e,g) Blood pressure profile and result of iHealth Lab Inc. for 1st, 2nd, 3rd, 4th week measurement, respectively. **(b,d,f,h)** Normalized average I_{DS} peaks of the sensor with respect to 1st week I_{DS} peaks over 15 s sensing period for 1st, 2nd, 3rd, 4th week measurement, respectively.
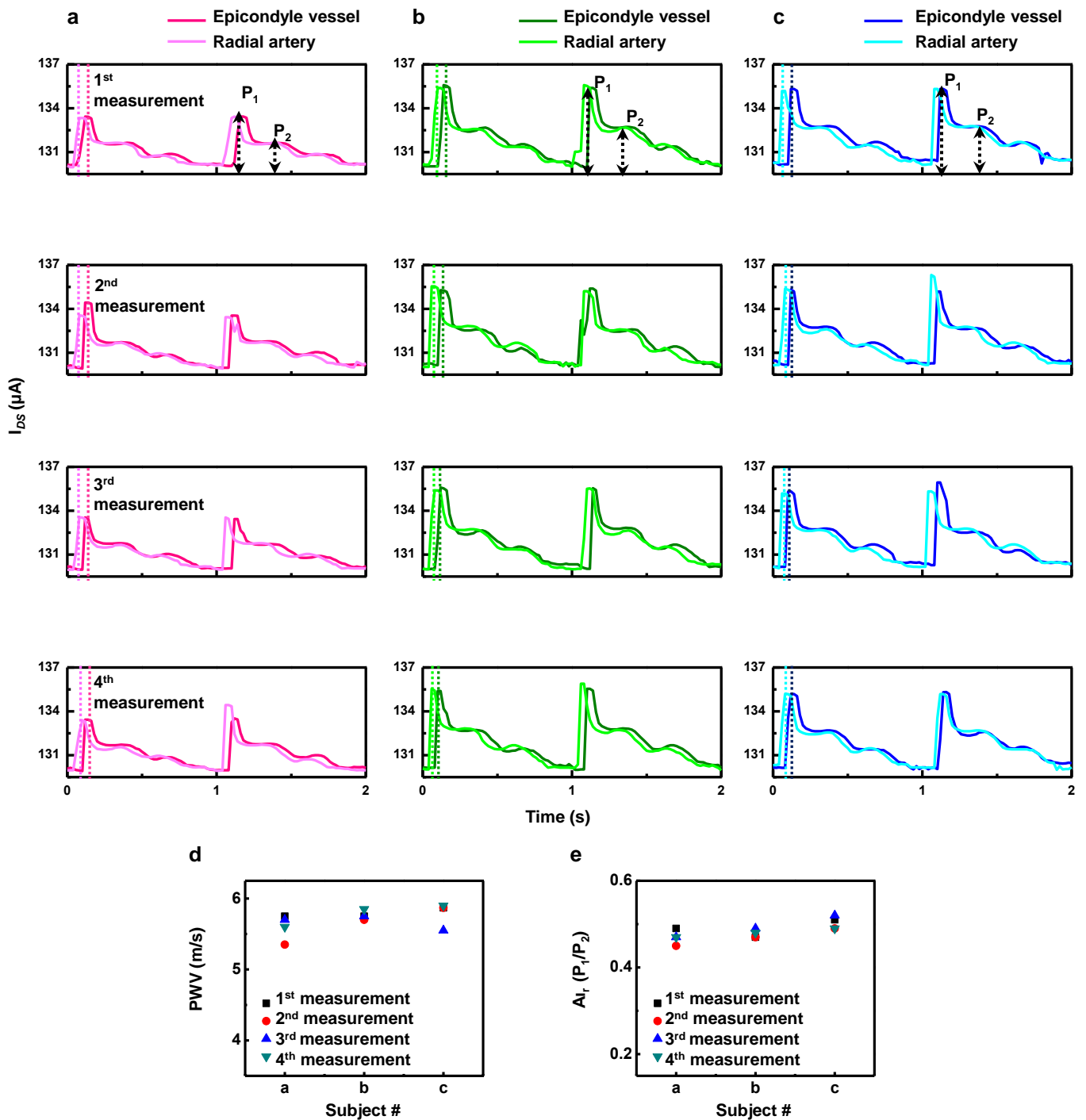
Supplementary Figure 17| Blood pressure wave monitoring over extended periods of time. **(a,b,c)** I_{DS} - Time plot for sensors placed on the lateral epicondyle vessel and radial artery of the wrist for 4 consecutive measurements collected from 3 human subjects: a, b, c. The time shifts of the initial peaks in the waveforms are indicated with dashed lines. Summary of results obtained in **a, b,** and **c** for **(d)** PWV, **(e)** the augmentation index (P_2/P_1).
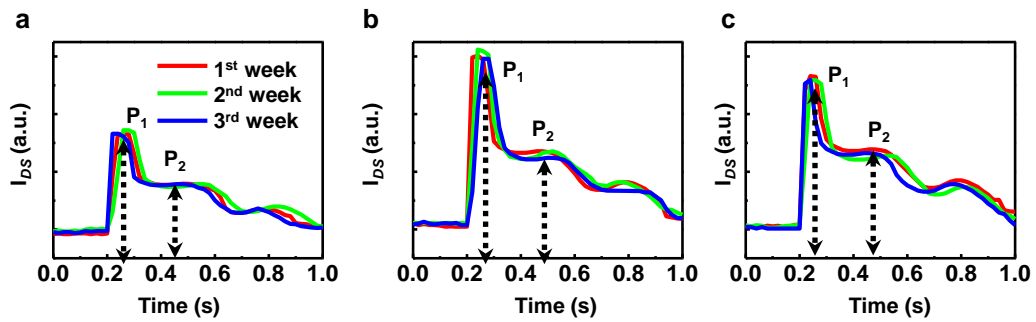
Supplementary Figure 18| Blood pressure wave monitoring over extended periods of time. (**a,b,c**) Normalized average I_{DS} response for ~10 single pulse measurements collected once per week for 3 weeks (red: 1st, green: 2nd, and blue: 3rd) for 3 subjects.
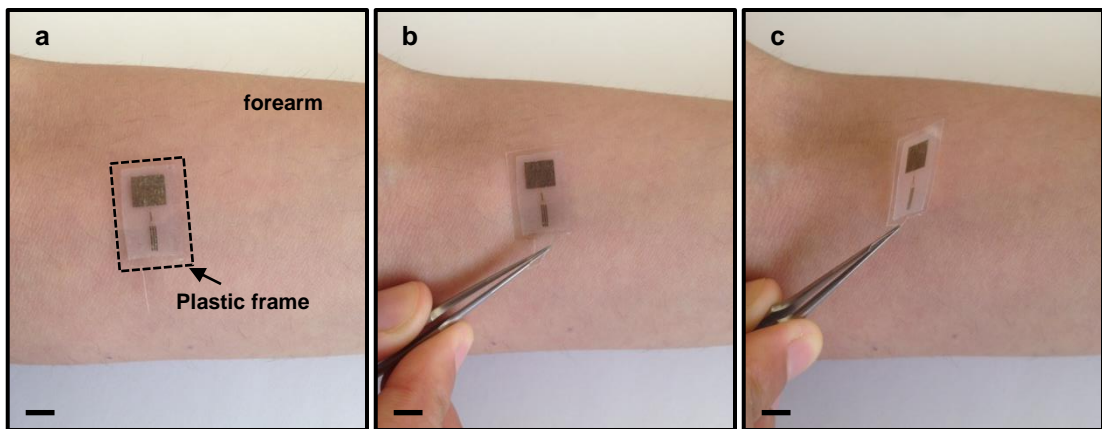
Supplementary Figure 19| Photographs of the process of mounting a device on the skin (a) and peeling it away (b, c). The scale bars are 1 cm.
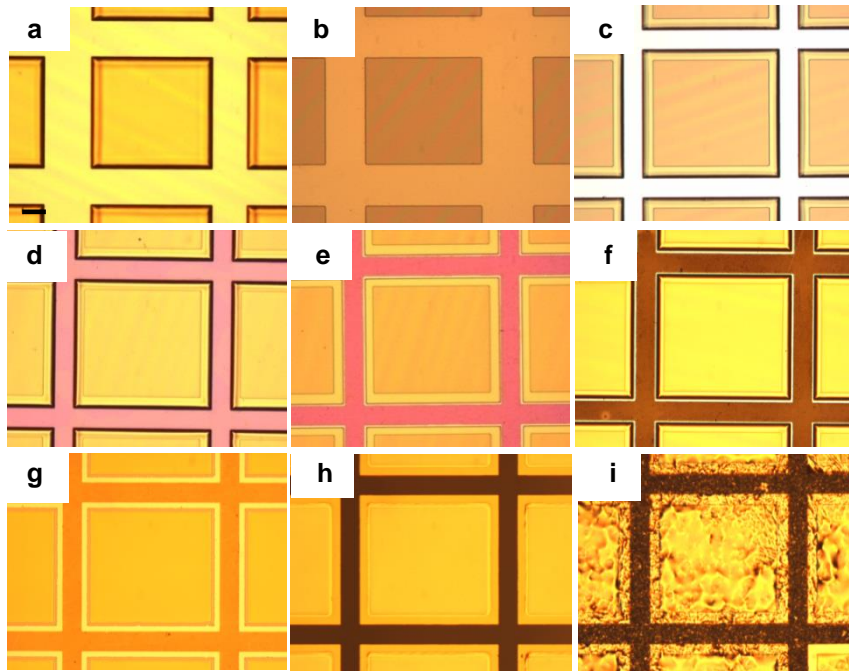
Supplementary Figure 20| Steps for fabricating arrays of PZT elements for pressure sensors. Optical microscope image of (**a**) photoresist patterning to defined regions for etching a layer of PZT, (**b**) pattern of PZT after etching, (**c**) photoresist patterning for etching the underlying layer of Pt, (**d**) Pt layer after selective etching, (**e**) photoresist patterning mask for undercuttting the SiO_2 layer with diluted HF, (**f**) pattern after etching with HF, (**g**) remaining materials on the silicon wafer after retrieving the PZT elements with a PDMS stamp, (**h**) PZT elements on the PDMS stamp, (**i**) PZT elements after printing onto a layer of silver epoxy on an extended gate electrode of a SiNM n-MOSFET. The scale bar is 100 μm.

a

Intensity (a.u.)

Pt (111)

Si (400)

PZT (111)

PZT (100) PZT (200)

Si

2 θ (deg)

b

Au/Cr

PZT

Pt/Ti

SiO$_2$

c

Polarization (μC/cm^2)

Voltage (V)
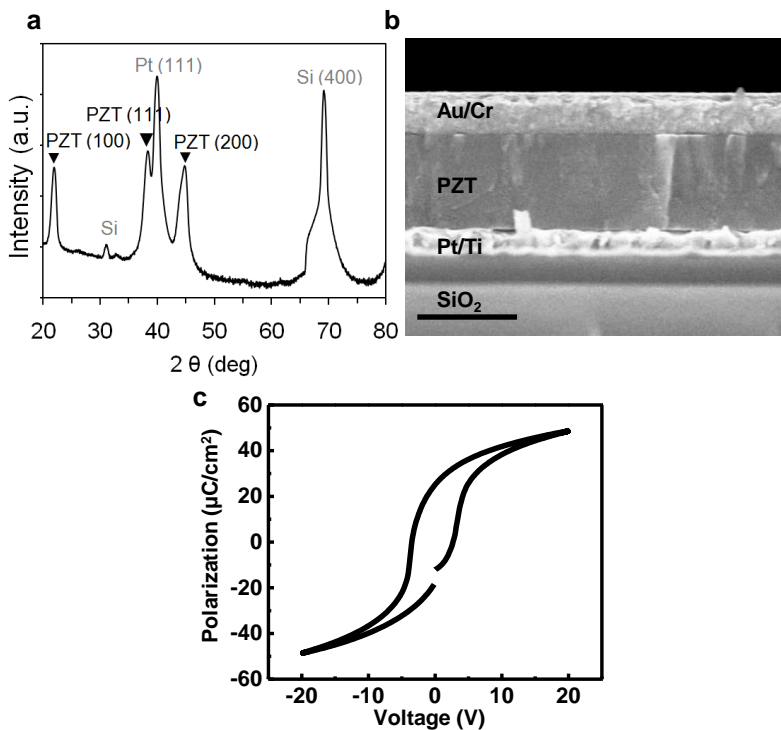
Supplementary Figure 21| Characterization of the PZT. (a) X-ray diffraction spectrum showing preferred orientation of PZT, through peaks labeled (100), (111) and (200). **(b)** SEM cross-sectional image of the materials stack, Au/Cr/PZT/Pt/Ti, on SiO$_2$/Si. The scale bar is 500 nm. **(c)** Polarization - Voltage plot for PZT thin film.
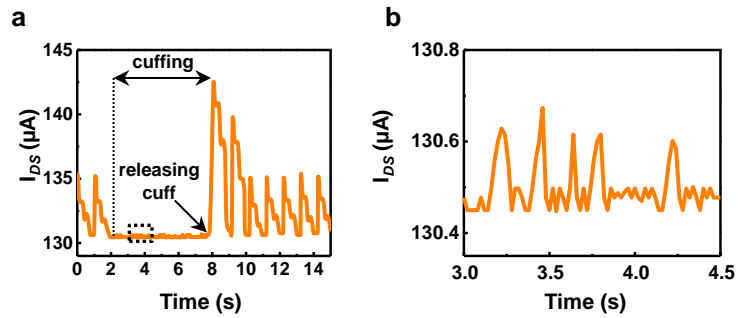
Supplementary Figure 22|Signal to noise ratio. (**a**) I_{DS} - Time plot for the sensor while reading pressure on the wrist before, during and after application of pressure on the arm using a commercial pneumatic cuff. (**b**) I_{DS} - Time plot of black dashed region of **a**.

a

CPRESS

- 5.00e-05
- 3.75e-05
- 2.50e-05
- 1.25e-05
- 0.00e+00

PDMS post

b

CPRESS

- 5.00e-05
- 3.75e-05
- 2.50e-05
- 1.25e-05
- 0.00e+00
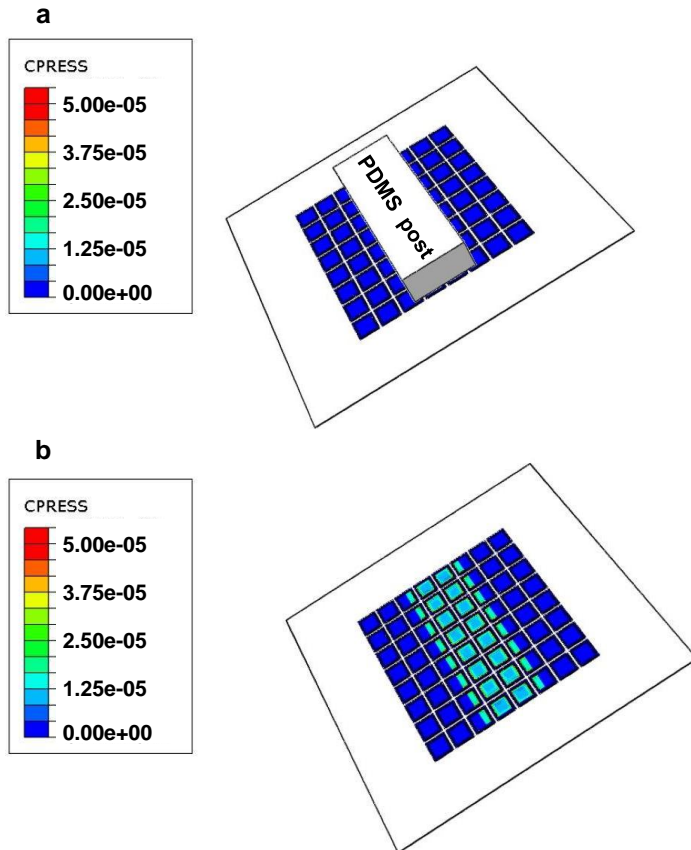
Supplementary Figure 23| Map of contact pressure. Calculated pressure associated with contact between a PDMS post (1 mm thick; in (**a**)) and an array of PZT elements on silicone (**b**).

Supplementary Tables

Supplementary Table 1| Capacitances of the n-MOSFET with 200 µm and 800 µm channel width.

Channel width (µm)	Material	Area A (m^2)	Thickness t (nm)	Dielectric Constant k (F m^-1)	Capacitance C (pF)
200	SiO$_2$ (ref. 2)	4×10^{-9}	140	3.90*8.85e-12	0.93
	Al$_2$O$_3$ (ref. 2)	4×10^{-9}	10	9.34*8.85e-12	
800	SiO$_2$ (ref. 2)	16×10^{-9}	140	3.90*8.85e-12	3.72
	Al$_2$O$_3$ (ref. 2)	16×10^{-9}	10	9.34*8.85e-12	

Supplementary Table 2| Summary of MIDI notes, pressure levels and sensor responses examined in the present work.

MIDI Note	Frequency (Hz)	Description	The Decibel (dB)	p_{rms} (Pa)	p_{peak} (Pa)	ΔI_{DS} (µA)
C1	32	Lowest C on a standard 88-key piano	49.6	0.00610	0.00863	5.08×10^{-3}
C2	65	Lowest note for Cello	64.9	0.0352	0.0498	2.67×10^{-2}
C3	130	Lowest note for viola, mandola	73.7	0.0970	0.137	1.25×10^{-1}
C4	261	Middle C	80.0	0.200	0.283	2.08×10^{-1}

The sensor used a SiNM n-MOSFET with channel width of 800 µm.

Supplementary Notes

Supplementary Note 1. The voltage of PZT layers array

The PZT formed on a silicon wafer (Young's modulus of 168 GPa) was released and then transfer printed onto silicone substrate (Young's modulus of 60 kPa) or another silicon wafer to form pressure sensors, according to detailed procedures described in the Methods. The PZT sensors were subjected to the weight of calibrated PDMS (density ~1 kg/m^3) posts with sizes of 6 mm$\times$2 mm$\times t_{PDMS}$, where t_{PDMS} is the thickness. Detailed layouts and related information can be found in Supplementary Figures 5a,b.

PZT is transversely isotropic with elastic, piezoelectric, and dielectric constants c_{ij}, e_{ij}, and k_{ij} (ref. 1), respectively. Standard constitutive models give relationships between the stress σ_{ij}, strain ε_{ij}, electric field E_i and electric displacement D_i as

$$\begin{Bmatrix} \sigma_{11} \\ \sigma_{22} \\ \sigma_{33} \\ \sigma_{23} \\ \sigma_{31} \\ \sigma_{12} \end{Bmatrix} = \begin{bmatrix} c_{11} & c_{12} & c_{13} & 0 & 0 & 0 \\ c_{12} & c_{11} & c_{13} & 0 & 0 & 0 \\ c_{13} & c_{13} & c_{33} & 0 & 0 & 0 \\ 0 & 0 & 0 & c_{44} & 0 & 0 \\ 0 & 0 & 0 & 0 & c_{44} & 0 \\ 0 & 0 & 0 & 0 & 0 & (c_{11}-c_{12})/2 \end{bmatrix} \begin{Bmatrix} \varepsilon_{11} \\ \varepsilon_{22} \\ \varepsilon_{33} \\ 2\varepsilon_{23} \\ 2\varepsilon_{31} \\ 2\varepsilon_{12} \end{Bmatrix} - \begin{bmatrix} 0 & 0 & e_{31} \\ 0 & 0 & e_{31} \\ 0 & 0 & e_{33} \\ 0 & e_{15} & 0 \\ e_{15} & 0 & 0 \\ 0 & 0 & 0 \end{bmatrix} \begin{Bmatrix} E_1 \\ E_2 \\ E_3 \end{Bmatrix}, \quad (1)$$

$$\begin{Bmatrix} D_1 \\ D_2 \\ D_3 \end{Bmatrix} = \begin{bmatrix} 0 & 0 & 0 & 0 & e_{15} & 0 \\ 0 & 0 & 0 & e_{15} & 0 & 0 \\ e_{31} & e_{31} & e_{33} & 0 & 0 & 0 \end{bmatrix} \begin{Bmatrix} \varepsilon_{11} \\ \varepsilon_{22} \\ \varepsilon_{33} \\ 2\varepsilon_{23} \\ 2\varepsilon_{31} \\ 2\varepsilon_{12} \end{Bmatrix} + \begin{bmatrix} k_{11} & 0 & 0 \\ 0 & k_{22} & 0 \\ 0 & 0 & k_{33} \end{bmatrix} \begin{Bmatrix} E_1 \\ E_2 \\ E_3 \end{Bmatrix}. \quad (2)$$

The PZT sensor consists of a square array of square elements of PZT structures connected in parallel by sharing top (and bottom) electrodes. Voltages develop between the top and bottom electrodes when the PZT is under compression.

For the voltage measurement on the hard silicon substrate, the PZT undergoes simple compression along the thickness direction due the weight of the PDMS post. The strains along other directions are approximately zero because of the constraint of the silicon substrate. Therefore, the constitutive model gives

$$-P = c_{33}\varepsilon_{33} - e_{33}E_3$$
$$D_3 = e_{33}\varepsilon_{33} + k_{33}E_3 \text{,}$$

(3)

where P is the pressure from the PDMS post. Elimination of ε_{33} gives $D_3 = -\left(e_{33}/c_{33}\right)P + \left(k_{33} + e_{33}^2/c_{33}\right)E_3$. The array of PZT structures, some fraction of which contacts the PDMS post, can be separately considered as regions that are and are not in contact with the PDMS, as $A_{contact}$ and $A - A_{contact}$, where A is the total area of PZT structures, as shown in Supplementary Figures 5c-g. The two regions are at the same voltage V because they share the same electrode. For the contacting region, the governing equation becomes

$$\frac{Q}{A_{contact}} = -\frac{e_{33}}{c_{33}}P + \left(k_{33} + \frac{e_{33}^2}{c_{33}}\right)\frac{V}{t_{PZT}},$$

(4)

where Q is the charge on the contacting region and t_{PZT} is the thickness of PZT. The total charge of the two regions is zero, which gives the governing equation for the non-contact part as

$$-\frac{Q}{A - A_{contact}} = \left(k_{33} + \frac{e_{33}^2}{c_{33}}\right)\frac{V}{t_{PZT}},$$

(5)

where the pressure on the non-contacting region is zero. Elimination of Q from equations (4) and (5) gives the voltage as

$$V = \frac{e_{33}t_{PZT}A_{contact}P}{A\left(k_{33}c_{33} + e_{33}^2\right)}. \tag{6}$$

For PZT with the elastic constants $\{c_{11}, c_{12}, c_{13}, c_{33}, c_{44}\}$ = {101, 77.8, 158, 82.2, 25.6} GPa, piezoelectric constants $\{e_{13}, e_{33}, e_{15}\}$ = {-14.8, 10.0, 13.4} C m^-2, and dielectric constants $\{k_{11},$ $k_{33}\}$ = {6.00, 2.57} nC/(Vm) (ref. 1), $t_{PZT} = 400\,\mathrm{nm}$, $A_{contact} = 2 \times 6\,\mathrm{mm}^2$ and $A = 64 \times 0.625 \times 0.557\,\mathrm{mm}^2$ as in the experiment, the analytical result according to equation (6) agrees well with the FEM results (Supplementary Figure 4) and experiment results (Fig. 2a).

Supplementary Note 2. The capacitance

The capacitance is given by

$$C = k\frac{A}{t}, \tag{7}$$

where k is the dielectric constant, A is the area, and t is the thickness of the capacitor. For the PZT structures, A = 22.28 mm^2, $t = 400\,\mathrm{nm}$, and k = 2.57 nC V^-1 m^-1, which gives a capacitance of $C = 0.14\,\mathrm{\mu F}$.

The SiNM n-MOSFET is operated in an active mode, for which a conductive channel exists between the drain and the source. The capacitance approximately equals that of the gate oxide (bilayer structure consisting of 140 nm silicon dioxide (SiO$_2$) with 10 nm aluminum oxide (Al$_2$O$_3$) above and below, where Al$_2$O$_3$ is in contact with the SiNM. For such a series connection, the capacitance is given as

$$\frac{1}{C_{Gox}} = \frac{1}{C_{Al_2O_3}} + \frac{1}{C_{SiO_2}} + \frac{1}{C_{Al_2O_3}}, \tag{8}$$

where $C_{Al_2O_3}$ and C_{SiO_2} are the capacitances of the Al_2O_3 and SiO_2 layers, respectively. Supplementary Table 1 gives the size and dielectric constants of the n-MOSFET with 800 μm channel width and the calculated capacitances by equation (8).

The device circuit (Fig. 1c) involves PZT capacitor in series with the gate oxide capacitance of the SiNM n-MOSFET. For such a series connection, the modulation of the gate bias (ΔV_{GS}) induced by applied pressure is related to the compensating surface charge δq. Since the PZT structures are connected to the gate of the SiNM n-MOSFET, redistribution of surface charges on the application of external pressure appears as a voltage signal to the gate (ΔV_{GS}) that is amplified by the SiNM n-MOSFET. The magnitude of ΔV_{GS} is obtained from equations (1) and (2) and the model for the device circuit in Fig. 1c.

Supplementary Note 3. Properties of the SiNM n-MOSFETs

The I_{DS} can be written by

$$I_{DS} = \begin{cases} \dfrac{\mu k}{2T} \dfrac{W}{L} (V_{GS} - V_{in})^2 & V_{GS} - V_{in} < V_{DS} \quad Saturated\ State \\ \dfrac{\mu k}{2T} \dfrac{W}{L} \left[2(V_{GS} - V_{in})V_{DS} - V_{DS}^2 \right] & V_{GS} - V_{in} > V_{DS} \quad Non-Saturated\ State \end{cases} \tag{9}$$

where μ is the electron mobility, T, W and L are the thickness of channel, the transistor effective gate width and length, respectively, and $k = 1/\left(x_{SiO_2}/k_{SiO_2} + x_{Al_2O_3}/k_{Al_2O_3} \right)$ is the effective dielectric constant for sandwich structure of Al_2O_3 and SiO_2 (ref. 3) with volume fractions $x_{SiO_2} = 0.875$ and $x_{Al_2O_3} = 0.125$ and dielectric constants k_{SiO_2}, $k_{Al_2O_3}$ as seen in Supplementary Table 1. The increment of I_{DS} due to the change of V_{GS} becomes

$$\Delta I_{DS} = \begin{cases} \dfrac{\mu k}{2T}\dfrac{W}{L}\left[2\left(V_{GS}-V_{in}\right)\Delta V_{GS}+\Delta V_{GS}^2\right] & V_{GS}-V_{in}<V_{DS} \quad Saturated\ State \\[2ex] \dfrac{\mu k}{T}\dfrac{W}{L}V_{DS}\Delta V_{GS} & V_{GS}-V_{in}>V_{DS} \quad Non-Saturated\ State \end{cases} \qquad (10)$$

The non-saturated part of equation (10), which is the working range of our devices, gives a relation between ΔI_{DS} and ΔV_{GS} as shown in equation (3) in the main text with the transconductance gain

$$g_m = \frac{\mu k}{T}\frac{W}{L}V_{DS} \qquad (11)$$

The experiment results of the n-MOSFET with 200 µm and 800 µm channel width shown in Fig. 2d and Supplementary Figure 7g give g_m as 11.1µA V^-1 and 33.2µA V^-1, respectively. For $T=100\,\text{nm}$, $L=20\,\mu\text{m}$, and $k=3.72\times10^{-11}C$ V^-1 m^-1, the electron mobility μ are 322cm^2 V^-1 s^-1 and 241 cm^2 V^-1 s^-1 for the 200 µm and 800 µm channel width, which are within a reasonable range. V_{DS} is set at 0.1 V for all cases.

Supplementary Note 4. Calculating sound pressure

A digital sound level meter (Radio Shack, 33-2055) was used to measure the levels, in decibels (dB), of audible MIDI notes played by an iHM79 stereo speaker. Supplementary Table 2 summarizes the parameters for cases that were studied. The corresponding sound pressure is calculated according to equation (12),

$$p_{rms} = p_0 10^{\frac{L_p}{20}}\,(\text{Pa}) \qquad (12)$$

where p_0, reference sound pressure $p_0 = 20\,\mu\text{Pa}\equiv 0\,\text{dB}$ and L_p is the sound pressure level.

Supplementary Note 5. Bending analysis

As shown in Supplementary Figure 12a, the position of the neutral mechanical plane (NMP) is

$$y_{neutral} = \left[\sum_{i=1}^{8} E_i t_i \left(2\sum_{j=1}^{i} t_j - t_i \right) \right] \bigg/ \left(2\sum_{i=1}^{8} \bar{E}_i t_i \right) \tag{13}$$

where the summation is for all layers, E_i and t_i are the modulus and thickness of the ith layer, respectively. The distance from the NMP to the mid-plane of PZT is

$$h = \sum_{i=1}^{6} t_i + \frac{t_7}{2} - y_{neutral} \tag{14}$$

For the structure shown in Supplementary Figure 12a, $E_1 = 60.0\,\text{kPa}$ and $t_1 = 20\,\mu\text{m}$ for silicone, $E_2 = 2.50\,\text{GPa}$ and $t_2 = 1.2\,\mu\text{m}$ for the PI layer, $E_3 = 279\,\text{GPa}$ and $t_3 = 10\,\text{nm}$ for Cr, $E_4 = 79\,\text{GPa}$ and $t_4 = 150\,\text{nm}$ for Au, $E_5 = 116\,\text{GPa}$ and $t_5 = 20\,\text{nm}$ for Ti, $E_6 = 168\,\text{GPa}$ and $t_6 = 150\,\text{nm}$ for Pt, $E_7 = 60.0\,\text{GPa}$ and $t_7 = 400\,\text{nm}$ for PZT, and $E_8 = 2.50\,\text{GPa}$ and $t_8 = t_{PI}$ for PI; these give the distance h decreasing with the increase of the top PI thickness (t_{PI}) as shown in Fig. 3d. For the top PI layer thickness $t_{PI} = 3.6\,\mu\text{m}$ as in the experiment, the NMP is very close to the middle plane of the PZT layer, with their distance only $h = 1.19$ nm. Without the top PI layer ($t_{PI} = 0$) the distance h increases by two orders of magnitude to $h = 259$ nm, which is larger than the half thickness (200 nm) of PZT such that the NMP is out of the PZT layer. Supplementary Figure 12b shows that, without the top PI layer, the linear relation between $\Delta I_{DS,pressure}$ and P still holds, though the slope in Supplementary Figure 12b is ~10% larger than that in Fig. 3e.

Let $EI_{spacing} = E_1 t_1^3/12$ and $EI_{PZT} = \sum_{i=1}^{8} E_i t_i \left[t_i^2/3 + \left(\sum_{j=1}^{i} t_j - y_{neutral} \right) \left(\sum_{j=1}^{i} t_j - y_{neutral} - t_i \right) \right]$

denote the bending stiffness of silicone substrate without and with the PZT layers array printed

on its top, respectively. The length and spacing of PZT layers array are denoted by L_{PZT} and

$L_{spacing}$, respectively. The corresponding radii of curvature R_{PZT} and $R_{spacing}$ are related by the

continuity of bending moment as $EI_{PZT}/R_{PZT} = EI_{spacing}/R_{spacing}$. The angle of rotation due to

bending $L_{PZT} R_{PZT}^{-1} + L_{spacing} R_{spacing}^{-1}$ is related to the effective radius R by $\left(L_{PZT} + L_{spacing} \right) R^{-1}$.

These relations give

$$R_{PZT} = \eta R. \tag{15}$$

where

$$\eta = \frac{L_{PZT} + \dfrac{EI_{PZT}}{EI_{spacing}} L_{spacing}}{L_{PZT} + L_{spacing}}. \tag{16}$$

The membrane strain in PZT is the strain at its mid-plane, and is given by

$$\varepsilon_{PZT} = \frac{h}{\eta R}. \tag{17}$$

Supplementary Note 6. Effects of bending on I_{DS}

For PZT subject to in-plane stretching (i.e., applied strain ε_{PZT}) along x_1 direction and

vanishing strain in the perpendicular, x_2 direction (constrained by the substrate), the constitutive

model, together with the vanishing stress in the normal (poling), x_3 direction, give

$D_3 = \bar{e} \varepsilon_{PZT} + \bar{k} E_3$, where $\bar{e} = e_{31} - \left(c_{13}/c_{33} \right) e_{33}$ and $\bar{k} = k_{33} + e_{33}^2/c_{33}$ are effective piezoelectric

and dielectric constants calculated by the elastic, piezoelectric and dielectric constants given in Supplementary Note 1, respectively. The open circuit condition (D_3=0), together with $E_3 = V_{PZT}/t_{PZT}$, give the voltage as

$$V_{PZT} = -\frac{\overline{e}}{\overline{k}} t_{PZT} \varepsilon_{PZT} . \tag{18}$$

Equations (2) and (3) in the main text and equations (17) and (18) give $\Delta I_{DS,bending}$ in equation (5) in the main text.

Supplementary References

1. Yang, J. & Yang, J.S. *An Introduction to the Theory of Piezoelectricity*. (Springer Science + Business Media, Inc., Boston, 2005).

2. Robertson, J. High dielectric constant oxides. *Phys. J. App. Phys.* **28,** 265-291 (2004).

3. Petrovsky, V., Jasinski, P. & Dogan, F. Effective dielectric constant of two phase dielectric systems. *J. Electroceram.* **28,** 185–190 (2012).